Chinese Journal of Natural Medicines

Pulchinenoside B4 attenuates gouty arthritis by regulating NLRP3 inflammasome and macrophage polarization: a transcriptomics-based analysis

Zitong Zheng, Shang Lyu, Meijuan Wang, Peng Liu, Yashi Ou, Junfang Yi, Huajie Yang, Zengrui Liao, Jiangting Sun, Wei Zou, Yulin Feng

Citation: Zitong Zheng, Shang Lyu, Meijuan Wang, Peng Liu, Yashi Ou, Junfang Yi, Huajie Yang, Zengrui Liao, Jiangting Sun, Wei Zou, Yulin Feng, Pulchinenoside B4 attenuates gouty arthritis by regulating NLRP3 inflammasome and macrophage polarization: a transcriptomics-based analysis, Chinese Journal of Natural Medicines, 2026, 24(4), 440-453. doi: 10.1016/S1875-5364(26)61173-9.

View online: https://doi.org/10.1016/S1875-5364(26)61173-9

Chinese Journal of Natural Medicines 24 (2026) 440-453

Contents lists available at ScienceDirect

Chinese Journal of Natural Medicines

journal homepage: www.cjnmcpu.com/

Original article

Pulchinenoside B4 attenuates gouty arthritis by regulating NLRP3 inflammasome and macrophage polarization: a transcriptomics-based analysis

Zitong Zheng[a,Δ], Shang Lyu[a,b,Δ*], Meijuan Wang[a], Peng Liu[a,b], Yashi Ou[a], Junfang Yi[a], Huajie Yang[a,b], Zengrui Liao[a], Jiangting Sun[a], Wei Zou[a], Yulin Feng[a,b,*]

[a] *School of Pharmacy, Jiangxi University of Chinese Medicine, Nanchang 330004, China*
[b] *National Pharmaceutical Engineering Center for Solid Preparation in Chinese Herbal Medicine, Nanchang 330006, China*

ARTICLE INFO

Article history:
Received 12 September 2025
Revised 21 December 2025
Accepted 19 February 2026
Available online 20 April 2026

Keywords:
Transcriptomics
Gouty arthritis
Pulchinenoside B4
NLRP3 inflammasome
Macrophage polarization
Nuclear factor-κB

ABSTRACT

Gouty arthritis (GA) is an inflammatory disorder characterized by the deposition of monosodium urate (MSU) crystals in joint tissues. Pulchinenoside B4 (B4) has broad-spectrum anti-inflammatory properties, but its role and potential mechanism in the pathogenesis of GA are still unclear. The purpose of this study is to comprehensively elucidate the therapeutic effect and mechanism of B4 on GA by integrating transcriptome analysis and *in vitro* and *in vivo* experiments. In the MSU-induced mouse GA model, B4 treatment significantly improved ankle edema and reduced inflammatory cell infiltration. Through the analysis of transcriptome sequencing results, we identified multiple differentially expressed long non-coding RNAs (lncRNAs), such as *Nod1*, *Rbck1* and *Pycard*. In the in-depth exploration of the mechanism, we focused on the NOD-like receptor signaling pathway, NF-κB signaling cascade, and B4-regulated macrophage polarization. *In vitro* and *in vivo* models, we confirmed that B4 significantly inhibited the expression and activation of key components of NLRP3 inflammasome (such as ASC, Caspase-1 and IL-1β) by qPCR, Western blot and immunofluorescence. Flow cytometry and immunofluorescence analysis further showed that B4 could prevent MSU-induced macrophage polarization to pro-inflammatory M1 phenotype.Based on these results, this study elucidated the mechanism of B4 improving MSU-induced GA inflammatory response by inhibiting NLRP3 inflammasome activation and blocking M1 macrophage polarization. These results suggest that B4 has great potential as a candidate drug for the treatment of GA.

1. Introduction

GA is essentially an inflammatory response caused by MSU crystal deposition. This reaction is self-limited, mainly involving adjacent joints and soft tissues [1]. One of its characteristics is that MSU crystals are deposited on the surface of synovial epithelial cells. On the one hand, MSU crystals activate local macrophages, thereby triggering GA, which in turn promotes inflammatory signal transduction and immune cell recruitment; on the other hand, this cascade reaction leads to the release of pro-inflammatory mediators (such as IL-1β) and chemokines, and triggers the rapid infiltration of pro-inflammatory leukocytes (such as neutrophils and monocytes). Monocytes play a key role in the acute immune response and have multiple functions in anti-inflammatory and tissue repair processes [2]. Under physiological conditions, the function of monocytes is to supplement the number of macrophages in tissues; when tissue inflammation occurs, monocytes can quickly sense inflammatory signals, and then proliferate or differentiate into macrophages to coordinate the immune response. The latest evidence shows that macrophages not only participate in the formation of GA, but also play a central role in the process of disease progression and regression [3, 4].

Macrophages, as an important part of the innate immune system, play a crucial role in the pathogenesis of GA. When macrophages are exposed to various microenvironment signals, they will polarize, form two phenotypes, M1 and M2, and secrete various cytokines. In the acute inflammation stage of GA, M1 polarization is dominant, while in the remission stage, M2 polarization is dominant [5]. The dynamic changes of macrophage polarization are closely related to the development of chronic inflammation, metabolic disorders and autoimmune diseases. New evidence shows that M1/M2 phenotypic polarization plays a central role in the pathogenesis of macrophage-mediated GA. Specifically, activation of inflammatory NLRP3 in macrophages significantly enhanced the inflammatory response caused by MSU. In contrast, inhibition of this pathway can effectively reduce the production of IL-1β, thereby reducing the frequency and severity of GA seizures [6, 7]. By interfering with the polarization process of macrophages and the activation of NLRP3 inflammasome, it can inhibit the production of IL-1β and TNF-α. If this strategy is adopted, it may become a potential effective method for the treatment of GA.

* Corresponding author.
E-mail addresses: 20201013@jxutcm.edu.cn (S. Lyu); fengyulin2003@126.com (Y. Feng)
Δ These authors contributed equally to this work.

https://doi.org/10.1016/S1875-5364(26)61173-9

In the treatment of gouty arthritis, the main drugs used in clinical practice are still limited to several types. One is colchicine, the second is non-steroidal anti-inflammatory drugs (NSAIDs), and the third is glucocorticoids. Although the therapeutic effect of these drugs is quite significant, but often accompanied by some adverse reactions. For example, long-term use may lead to drug resistance, or inhibit the body's own hormone synthesis process. In addition, they may also cause gastrointestinal irritation. It is worth noting that, on the one hand, with the deepening of research, people's understanding of the pathogenesis of GA is increasingly thorough; on the other hand, traditional Chinese medicine (TCM) such as Si Miao Decoction [8], Resveratrol [9], and Si Miao San [10] have been shown to have a significant effect on improving GA progression. Natural medicines have always occupied a central position in modern drug research and continue to promote the progress of research on the treatment of various human diseases [11]. The main pharmacodynamic component B4 of *Pulsatilla chinensisis* obtained *via* a systematic extraction and purification process of medicinal compounds from *Pulsatilla chinensis* herbs. First, *Pulsatilla chinensis* was processed to prepare standardized herbal tablets for subsequent refined use. The component B4 extracted from it has been proved to have a wide range of biological activities, including anti-tumor, anti-inflammatory, anti-virus, kidney protection, analgesia and immune regulation, and has multiple functional properties. In recent years, a large number of studies have explored the anti-inflammatory, immunomodulatory and anti-tumor activities of B4. Based on the results of various studies, it is consistent that B4 has good safety characteristics [12–14]. Our previous studies have also confirmed that B4 has a significant improvement effect on GA disease, which is characterized by rapid onset, high safety and protection of immune function. Compared with western drugs, B4 shows irreplaceable unique advantages, which highlights its important scientific research value.

However, to date, the specific mechanism by which B4 exerts beneficial effects on GA remains unclear. Therefore, this study established a MSU-induced GA model, combined with transcriptome sequencing technology and experimental verification. By systematically studying the mechanism of B4 alleviating GA, the final research results provide a more comprehensive experimental basis for the future application of B4 in GA treatment to achieve multi-pathway and multi-target combination therapy.

2. Materials and methods

2.1. Reagents and chemicals

Monosodium urate purchased from Sigma-Aldrich (St. Louis, MO, USA). Diclofenac sodium is from Shanghai Aladdin Biochemical Technology Company Limited. Fetal bovine serum (FBS) was purchased from Gibco (Scoresby, Australia). The decalcification solution was purchased from Biosharp Life Sciences, China. TRIzol reagent was purchased from Beijing All Style Gold Biotechnology Company Limited. The reverse transcription PCR kit and SYBR real-time quantitative fluorescence (qPCR) kit were purchased from Next Sense Biotechnology (Shanghai) Company Limited. BCA protein assay kit, protease inhibitor and phosphatase inhibitor were purchased from Jiangsu Kangwei Century Biotechnology Company Limited. PVDF membranes were purchased from milipore. iNOS (ab 178945), NLRP3 (ab 263899), Caspase-1 (ab 207802), and IL-1β (ab 254360) antibodies were purchased from Abcam, p-NF-κB (3033T) was purchased from Cell Signaling Technology, USA. ASC (10500-1-AP) antibody was purchased from Wuhan Three Eagles Biotechnology Company Limited. SuperSignal™ West Pico PLUS chemiluminescent substrate was purchased from Thermo, USA.

2.2. B4 extraction and purification

In this study, the B4 utilized was isolated by our research group from the rhizomes of *Pulsatilla chinensis* (Bunge) Regel, with a purity exceeding 98%. The structure of B4 was verified by means of ultra-performance liquid chromatography-time-of-flight mass spectrometry (UPLC-Q-TOF-MS), nuclear magnetic resonance (NMR), ultraviolet (UV) spectroscopy, and infrared (IR) spectroscopy. Simultaneously, the content of B4 was calibrated.

Preparation process of B4 monomer: take the appropriate amount of Bactrianthus saponins, add 10 times the amount of 70% ethanol reflux extraction twice, each time for 2 h, combined extract, concentrated to no alcohol flavor, adsorbed by AB-8 macroporous resin column, in turn, with 2–3 BV water, 70% ethanol, 70% ethanol eluent was collected, concentrated to no alcohol, and then the liquid phase was prepared by Dynamic Axial HPLC to 50%–55% methanol water and 25%–30% acetonitrile water as the mobile phase for separation and purification, collected the content greater than 98% of the stream fraction, that is, B4 monomer. 30% acetonitrile water as the mobile phase for separation and purification, collect the content of more than 98% of the flow fraction, after concentration, dewatering, drying under reduced pressure, that is, the albizia saponin B4 monomer.

2.3. Preparation of MSU crystals

To prepare MSU crystals, 1 g of uric acid and 0.5 g of sodium hydroxide were dissolved in 100 mL of ddH_2O. The resultant solution was heated to 80 °C and maintained at this temperature for 20 min to ensure complete dissolution. Subsequently, the solution was allowed to crystallize overnight at 4 °C. The pH of the solution was then adjusted to 7.2 using dilute hydrochloric acid. Following this, the MSU crystals were harvested *via* centrifugation, extensively washed with deionized water to remove impurities, and finally dried at 80 °C for 24 h under controlled conditions.

2.4. Cell culture

The human-derived monocytic leukemia cell line, THP-1 cells, were cultured in RPMI-1640 medium supplemented with 10% FBS. The cultures were maintained at 37 °C in a humidified incubator with an atmosphere of 5% CO_2. THP-1 cells in the logarithmic growth phase were differentiated into macrophages by treatment with 150 ng·mL^{-1} phorbol 12-myristate 13-acetate (PMA) for 48 h.

2.5. Cell viability

The effects of B4 and diclofenac sodium on the viability of THP-1 cells were assessed using the CCK-8 assay. THP-1 cells were suspended at a concentration of 1×10^5 cells/mL, and 100 μL of the suspension was evenly distributed into each well of a 96-well plate. Subsequently, 100 μL of RPMI-1640 medium supplemented with 10% CCK-8 reagent was added to each well. The plate was incubated under standard conditions for 1–2 h. Finally, the OD value of the cells in each well was measured at 450 nm using a microplate reader, and cell viability was calculated based on these measurements.

2.6. Establishment of a GA model for MSU-induced THP-1 cells and pharmacological intervention

THP-1 cells in the logarithmic growth phase were harvested, resuspended in a cell suspension, centrifuged, and subsequently re-suspended for cell counting. The cells were then seeded into 6-well plates at a density of 1.5×10^6 cells/mL. Groups were ran-

domly assigned using the randomized numerical table method and included the following: normal control group, MSU model group, diclofenac sodium (50 μg·mL^{-1}) group, MUS + B4 (2.5 μg·mL^{-1}) group, MUS + B4 (5 μg·mL^{-1}) group, and MUS + B4 (10 μg·mL^{-1}) group. In this experiment, an MSU suspension at a concentration of 0.2 mg·mL^{-1} was utilized to establish the THP-1 inflammatory cell model, and THP-1 cells were collected after 24 hours of incubation.

2.7. Establishment and processing of mice GA model

5–6 week old male C57BL/6 mice (weighing 18–20 g) were procured from Henan Skebes Bio-technology Co., Ltd. (Certificate No.: SYXK 2022-0002). The animals were maintained in a controlled environment with a temperature of 23 ± 1 °C and relative humidity of 55% ± 5%. Prior to the experiment, the mice were acclimatized and provided standard chow for one week. Throughout the study, all mice had ad libitum access to food and water and were treated humanely in accordance with ethical guidelines. All experimental procedures adhered to the principles outlined in the Guide for the Care and Use of Laboratory Animals [National Institutes of Health (NIH), Bethesda, MD, United States] and were approved by the Laboratory Animal Ethics Committee of Jiangxi University of Traditional Chinese Medicine (Nanchang, China; License No.: ZLLSC20220188).

Sixty male C57BL/6 mice were randomly allocated into six groups (n = 10 per group): control, MSU, MSU + diclofenac sodium (11.25 mg·kg^{-1}), MSU + B4 (7.5 mg·kg^{-1}), MSU + B4 (15 mg·kg^{-1}), and MSU + B4 (30 mg·kg^{-1}). In the treatment groups, the corresponding drugs were administered intragastrically according to body weight (10 mg·kg^{-1}) starting 1 h prior to B4 modeling, with subsequent doses given every 3 h for a total of four administrations. Diclofenac sodium was administered once, 1 h before modeling. mice were anesthetized *via* intraperitoneal injection of pentobarbital sodium. Subsequently, 25 mg·mL^{-1} MSU suspension was subcutaneously injected into the dorsal side of the right ankle joint in both the model group and the treatment group, with a volume of 0.02 mL per mouse. The control group received an equivalent volume (0.02 mL) of sterile normal saline at the same site. This procedure established the GA model. Following successful injection, a visible swelling was observed on the contralateral side of the injection site. After 24 h, the skin and muscle tissues adjacent to the ankle joint were carefully excised along the line above the ankle joint. A portion of the ankle joint tissue was collected for histopathological examination, while the remaining tissue was stored at −80 °C for subsequent analyses.

2.8. Evaluation of ankle joint swelling in mice

Before MSU injection, a horizontal line was marked 5 mm above the ankle joint using an indelible marker to standardize the measurement of toe volume. Foot volume in mice was assessed *via* foot volumetry prior to modeling and at 1, 3, 6, 9, and 24 h post-modeling. The ankle swelling rate was calculated using the following formula: Ankle swelling rate (%) = $(b - a)/a \times 100\%$, where a represents the initial circumference of the joint, and b denotes the circumference of the joint after MSU crystal injection.

All of the aforementioned measurements were conducted in a blinded manner by the designated experimenter under controlled experimental conditions.

2.9. Hematoxylin and eosin (H&E) staining

Ankle tissue specimens were harvested and fixed in a 4% paraformaldehyde solution. Following fixation, the specimens underwent decalcification using an EDTA-based decalcification solution as part of the paraffin-embedding procedure. Subsequently, paraffin-embedded sections were stained with hematoxylin and eosin (H&E). Histopathological analysis was then performed using a panoramic slide scanner (3DHISTECH, Hungary).

2.10. Transcriptome of ankle joint

Total RNA was extracted using TRIzol™ Reagent. The purity of the RNA samples was assessed by measuring the OD260/280 ratio with a NanoDrop spectrophotometer, and the concentration was quantified using the Qubit 3.0 fluorometer. RNA integrity was evaluated using the Agilent Bioanalyzer 4200 system. Subsequently, 1 μg of total RNA was processed to remove ribosomal RNA using the Ribo-off rRNA Depletion Kit, followed by the construction of a strand-specific library with the VAHTS Universal RNA-Seq Library Prep Kit. Amplification products were purified using KAPA HiFi HotStart ReadyMix and VAHTS DNA Clean Beads. The library concentration was then measured using the Qubit®3.0 fluorometer, the fragment size distribution was analyzed using the Agilent 4200 TapeStation system, and the molar concentration of the library was determined by qPCR on the QuantStudio 5 platform. Finally, sequencing was performed on the Illumina NovaSeq X Plus instrument (San Diego, CA, USA) using the NovaSeq X Series 25B Reagent Kit (300 cycles; Catalog No. 20104706).

2.11. Differential expression LncRNA screening and data analysis

String software was used to count the raw sequence counts of known expressed LncRNAs, and the expression of known LncRNAs was calculated using FPKM to calculate the metrics, and DESeq R software was utilized to satisfy the $|\log_2 FC| \geq 1$ and $P \leq 0.05$ differential expression ranges to screen for differential LncRNAs between the control group *vs* the MSU group and the MSU group *vs* the B4 group . Volcano plots were used to show the distribution of differentially expressed LncRNAs between groups, heat maps to show clustering between groups, and finally GO functional analysis and KEGG enrichment analysis of common differentially expressed LncRNAs.

2.12. Molecular docking

The 3D structures of target proteins NLRP3, NF-κB and iNOS were downloaded from the PDB (http://www.rcsb.org/) database. CB-Dock2 database (http://clab.labsh are.co.uk/cb-dock/php.index.php) was adopted for protein-small molecule docking [15].

2.13. q-PCR

Total RNA was extracted from cells or tissues by following the instructions provided in the TRIzol reagent protocol, using TRIzol, chloroform, and isopropanol. The RNA concentration was subsequently determined by measuring the optical density at 260 nm after centrifugation of the supernatant. The purified RNA was stored at −80 °C for further analysis. Reverse transcription of the RNA into cDNA was performed using a reverse transcription kit in a 20 μL reaction volume. The resulting cDNA was used as a template for quantitative PCR (qPCR) analysis employing the SYBR Green I fluorescent detection method. The primer sequences utilized in this study are listed in Tables S1 and S2.

2.14. Western blot analysis

THP-1 cells and ankle tissues were harvested, lysed in RIPA buffer supplemented with 1% phosphatase inhibitor and protease inhibitor, and subsequently centrifuged at 4 °C for 10 min at 14 000 r·min^{-1} to collect the supernatants. The protein concentration was quantified using a BCA protein assay kit (CoWin Bi-

otech Co., Ltd., Jiangsu, China). Equal amounts of protein extracts were separated by SDS-PAGE and subsequently transferred onto PVDF membranes. The membranes were blocked with a protein-free rapid blocking solution, followed by incubation with primary antibodies against NLRP3, ASC, Caspase-1, IL-1β, iNOS, p-NF-κB, or β-actin on a shaker overnight at 4 °C. Afterward, the membranes were incubated with the corresponding secondary antibody for 1.5hours at room temperature and then visualized using enhanced chemiluminescence detection. The relative protein expression levels in each group were quantified using ImageJ analysis software, with β-actin serving as an internal reference.

2.15. Flow cytometry

THP-1 cells were immunostained with APC-conjugated anti-CD80 antibodies. Data acquisition was performed using a FACS Aria III flow cytometer (Beckman Coulter, Gallios, USA), followed by analysis using FlowJo software.

2.16. Immunofluorescence

Mice ankle joint tissues were collected, fixed with 4% paraformaldehyde, and subsequently decalcified. The tissues were then embedded in paraffin and sectioned. Paraffin sections were baked, rehydrated, and placed in a repair cassette for antigen retrieval using citric acid. Sections were permeabilized with 0.1% Triton X-100 at room temperature and blocked with 3% bovine serum albumin (BSA) for 1.5 h. The cells were subsequently subjected to immunostaining with an iNOS antibody (1∶100 dilution) and incubated overnight at 4 °C. This was followed by incubation with an Alexa Fluor-labeled secondary antibody (1∶300 dilution) for 1.5 h. Nuclear staining was performed using Hoechst for 5 minutes. Images were acquired using a LEICA laser confocal microscope (SP8 model).

2.17. Statistical analysis

The experimental data were statistically analyzed using SPSS statistical software (SPSS, Chicago, IL, USA), and the data were expressed as mean ± standard deviation , and comparisons between two groups were made using the two independent samples *t*-test, and comparisons between multiple groups were made using One-Way ANOVA, with $P < 0.05$ being considered as the statistically significant difference.

3. Results

3.1. Effect of B4 and diclofenac sodium on THP-1 cell viability

The THP-1 cell line has clear characteristics. It is an acute monocytic leukemia cell line, so it is widely used in many laboratories and can be regarded as an ideal model for studying immune response and inflammatory processes. Therefore, we selected THP-1 cell line to design subsequent experiments. Firstly, we used CCK-8 method to comprehensively evaluate the effects of B4 and diclofenac sodium on the viability of THP-1 cells in the concentration range of 0 to 1000 μg·mL^{-1}, and carefully analyzed these effects. As shown in Fig.1A, compared with the control group, B4 had no significant effect on cell viability in the concentration range of 0–1000 μg·mL^{-1}. However, when the cells were exposed to 1000 μg·mL^{-1} diclofenac sodium for 24 h, their viability was significantly inhibited ($P < 0.05$). Based on these results, it can be concluded that B4 had little effect on the proliferation of THP-1 cells within the test concentration range, while diclofenac sodium showed moderate cytotoxicity. Therefore, both compounds are suitable for subsequent experimental analysis.

3.2. B4 attenuates MSU crystal-induced inflammatory response in mice with gouty arthritis

Joint pain, stiffness, swelling, and intra-articular/periarticular inflammation are among the most common symptoms in MSU-related conditions. Compared with the control group, serum uric acid levels in MSU-injected mice were significantly elevated. Statistical analysis confirmed a significant difference in serum uric acid concentrations between the MSU and control groups ($P < 0.05$). However, compared with the MSU group, the low-, medium-, and high-dose groups treated with diclofenac sodium or B4 exhibited some inhibitory effect on serum uric acid levels. Notably, these reductions did not reach statistical significance (Fig. 1B). In order to evaluate the effect of B4 on the recovery process of GA, we closely observed the condition of mice. It was found that 24 hours after injection of MSU, the hind paws of mice showed symptoms of fever, redness and swelling, and the difference between the groups was statistically significant. Then we measured the swelling degree of these joints. The results showed that the ankle joint of mice showed progressive edema after administration of MSU. The ankle swelling ratio at each experimental time point after 6 hours of MSU injection was significantly higher than that of the control group ($P < 0.05$), confirming that the GA model was successfully established. It is worth noting that in the control group and the B4 group (30 mg·kg^{-1}), the ankle swelling ratio began to decrease significantly after reaching a peak at 3 hours. At 24 h, the swelling ratio of the MSU group continued to rise and peaked. In contrast, the degree of swelling in the B4 group was significantly lower than that in the MSU group. It is worth noting that compared with the positive control group treated with diclofenac sodium, the low-dose, medium-dose and high-dose B4 groups showed more significant short-term efficacy in inhibiting GA symptoms (Figs. 1C–1D).

To observe the state of tissue inflammation (Fig. 1E), we selected the ankle joints of mice and sliced them, followed by HE staining. Firstly, the synovial tissue structure of the control group remained intact, the cell morphology was normal, and no inflammatory cell infiltration was observed. Secondly, the MSU model group was completely different, the phenomenon of inflammatory cell infiltration was significant, and the pathological manifestations were extremely obvious. However, compared with the MSU model group, the positive drug group and the B4 group showed that the pathological changes in each group were significantly reduced. It is worth noting that the HE staining results of synovial tissue after high-dose B4 treatment were closer to those of the control group. Based on the above results, it can be clearly confirmed that B4 can not only effectively inhibit inflammatory cell infiltration, but also alleviate the progression of GA induced by MSU crystals in mice. Combining all the data, it can be further confirmed that B4 has a significant relief effect on GA symptoms induced by MSU crystals.

3.3. Effect of B4 on the transcriptome of the ankle joint in GA mice

Using $|\log_2 FC| > 1$ and $P < 0.05$ as filters, a total of 640 differentially expressed lncRNAs were identified between the blank and model groups, including *Cxcl1*, *Rbck1*, and *Ctsb*. Of these, 294 lncRNAs were up-regulated and 346 were down-regulated. In contrast, 2026 differentially expressed lncRNAs—such as *Atg12*, *Csnk2a2*, and *Pik3r2*—were detected between the model and B4 groups, with 1512 up-regulated and 514 down-regulated. The heatmap revealed a clear separation of differentially expressed lncRNAs between the B4 and model groups (Fig. 2A). To further characterize lncRNA expression changes in B4-treated GA, volcano plots were generated using DESeq2 software. As shown in

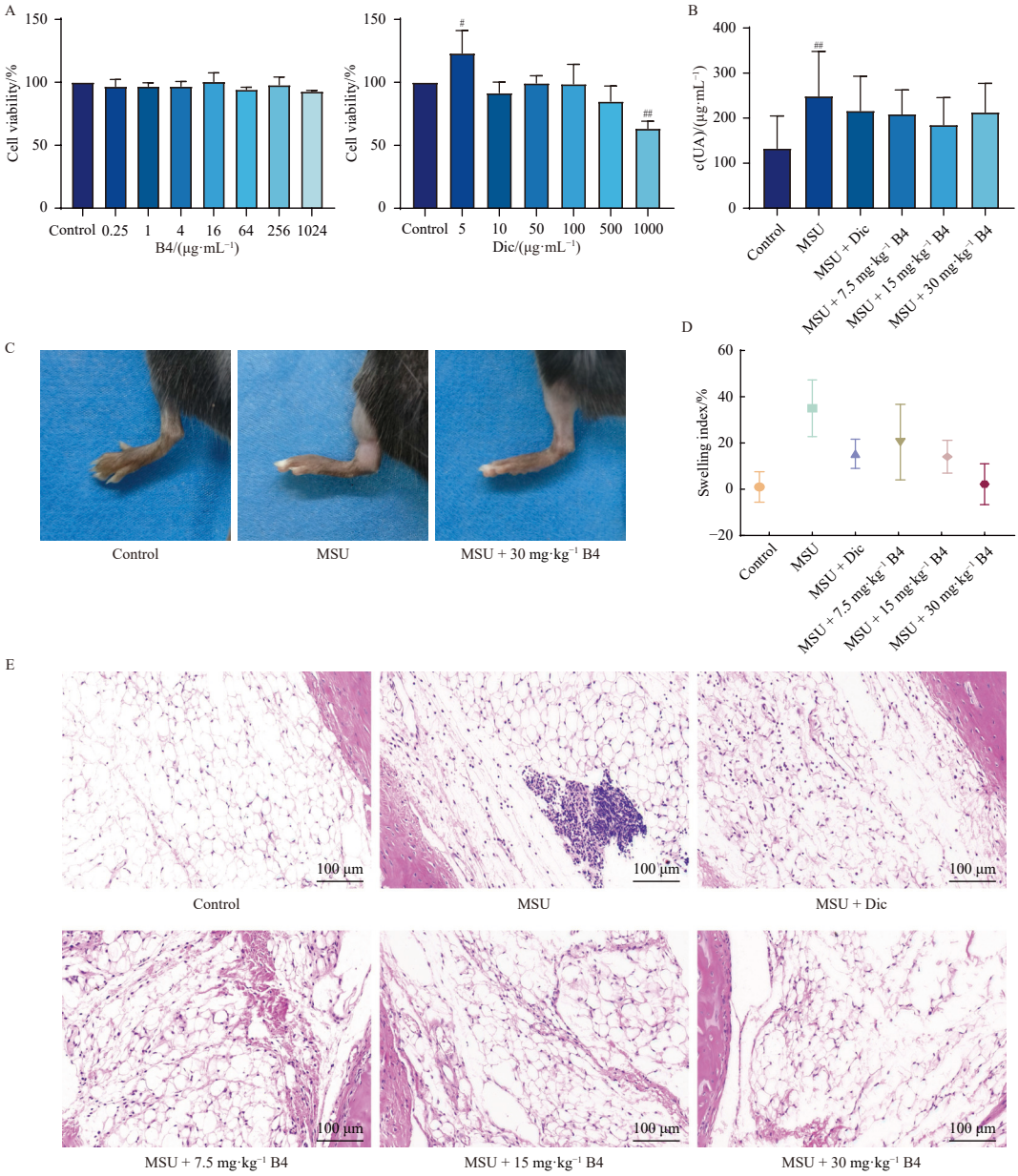

Fig. 1 B4 ameliorates MSU-induced inflammatory response in mice GA. (A) Effect of B4 and diclofenac sodium on THP-1 cell viability analyzed by CCK-8 assay. (B) Serum uric acid content in mice. (C) Pictures of swelling degree of the ankle joint in mice. (D) Analysis of the effect of B4 on the ankle Swelling rate in GA mice. (E) Photograph of H&E staining of synovial tissue of the ankle joint in GA mice (scale bar = 50 μm). Data are presented as means ± SD (n = 10). $^{\#}P < 0.05$, $^{\#\#}P < 0.01$, $^{\#\#\#}P < 0.001$ *vs* Control group; $^{*}P < 0.05$, $^{**}P < 0.01$, $^{***}P < 0.001$ *vs* MSU group.

the differential volcano plots, significant fold change differences in differentially expressed lncRNAs were observed between the blank and model groups, as well as between the model and B4 groups (Figs. 2B–2C).

To further clarify the GA mechanism and the biological functions of lncRNAs altered by B4 treatment in GA, this study performed GO functional enrichment analysis on 640 differentially expressed lncRNAs identified between the blank and model groups, as well as 2026 differentially expressed lncRNAs detected between the model and B4 groups. The results showed that differentially expressed lncRNAs in the blank *vs* model comparison were primarily enriched in functions such as cell growth regulation, xenobiotic stimulus response, signaling receptor activity modulation, and cytokine production involved in inflammatory responses (Fig. 2D). In contrast, differentially expressed lncRNAs in the model *vs* B4 comparison were mainly associated with processes like nuclear envelope organization, binding activities, muscle cell differentiation, and immune response-related cell activation (Fig. 2E).

The KEGG database was used to classify differentially expressed lncRNAs between the model and control groups, as well as between the B4 and model groups, *via* functional annotation and pathway enrichment analysis. A screening criterion of $P < 0.05$ was established, and the results were sorted based on the gene ratio. As illustrated in Fig. 2F, enrichment analysis of 640 differentially expressed lncRNAs identified between the control and model groups indicated their primary involvement in key signaling pathways, including the PI3K-Akt signaling pathway, NOD-like receptor signaling pathway and Toll-like receptor signaling pathway. First, we performed functional enrichment analysis of 2026 differentially expressed long non-coding RNAs (lncRNAs) in the model group and the B4 group. KEGG results showed that more signaling pathways were involved in the regulation process, including NOD-like receptor signaling pathway, TNF signaling pathway and TGF-β signaling pathway (Fig. 2G). Secondly, as shown in Fig. 2H, we used quantitative PCR to verify the mRNA expression levels of candidate lncRNA downstream target genes *Nod1*, *Rbck1* and *Pycard*. Compared with the control group, the

mRNA expression of *Nod1* and *Pycard* in the MSU group was significantly up-regulated, while the mRNA expression of *Rbck1* was significantly down-regulated. By comparing the B4 group and the MSU group, it was found that the expression of *Nod1* and *Pycard* mRNA was significantly inhibited after B4 treatment, while the expression of *Rbck1* mRNA was enhanced. Subsequently, we performed molecular docking analysis of B4 with key targets NLRP3, NF-κB, and iNOS. The analysis results show that the free binding energy range of the interaction is from −5.4 to −10.9 kcal·mol^{-1}, indicating that these key targets have good binding affinity with our core compounds (Fig. 2I). Therefore, based on these findings, in our study on GA, we carried out molecular biology experiments to further explore how B4 affects the mechanism of action of key components in the NOD-like receptor signaling pathway, including NLRP3, ASC, Caspase-1, NF-κB, IL-1β and TNF-α.

3.4. B4 inhibits MSU-induced activation of NLRP3 inflammatory in THP-1 cells

The activation of NLRP3 inflammasome plays a key role in the inflammatory response induced by MSU crystals. NLRP3 (NOD-like receptor hot protein domain-associated protein 3) is the core component of the NOD-like receptor family. The NLRP3 inflammasome complex is composed of NLRP3, apoptosis-associated speck-like protein ASC and Caspase-1. To elucidate this mechanism, we used qPCR to detect the mRNA expression levels of NLRP3 and Caspase-1. First of all, compared with the control group, the mRNA expression of *NLRP3* and *Caspase-1* in the model group was significantly increased ($P < 0.05$). Secondly, in THP-1 cells treated with MSU, the mRNA expression of *NLRP3* and *Caspase-1* in the model group could be significantly inhibited by B4

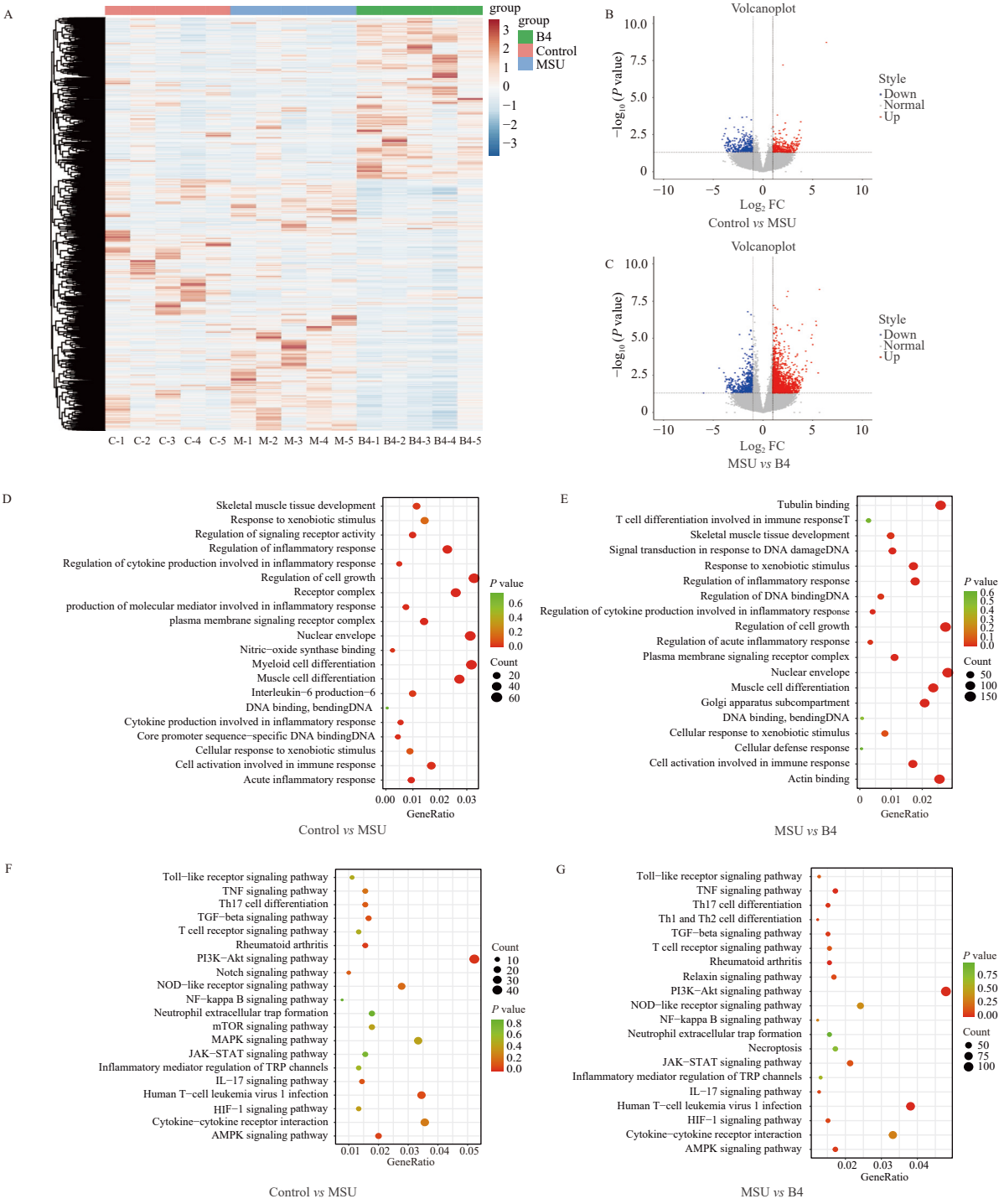

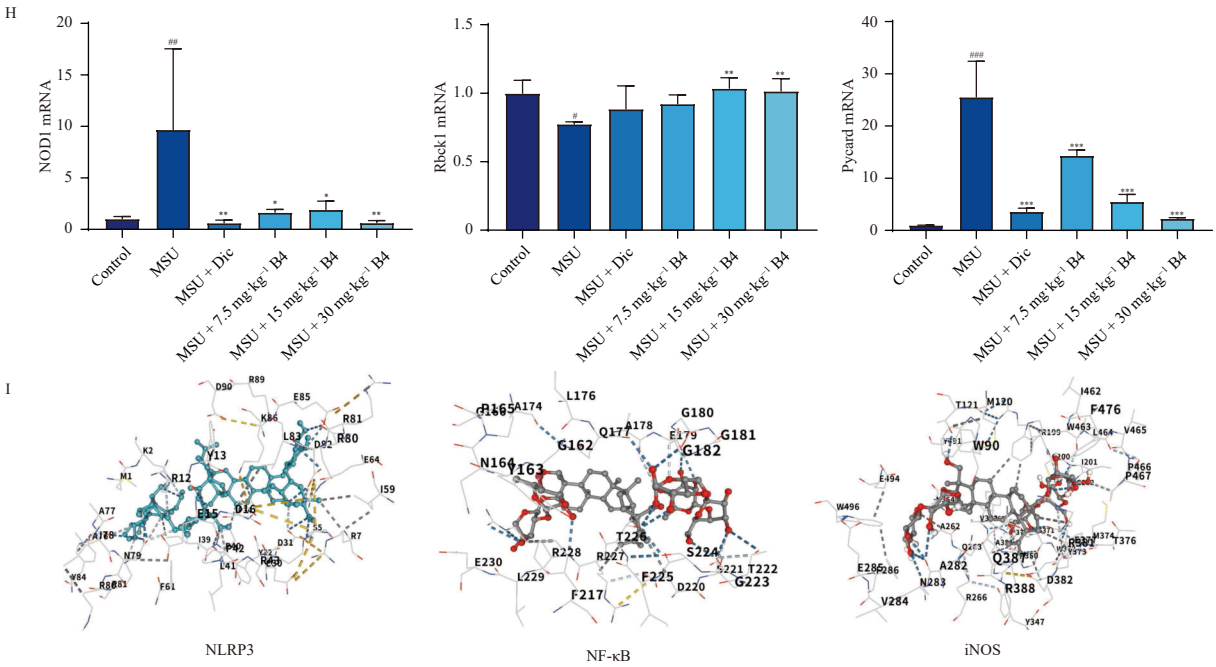

Fig. 2 Effect of B4 on the transcriptome of MSU-induced GA mice. (A) Cluster analysis of differentially expressed lncRNA between groups. (B) Volcano plot of differentially expressed lncRNA in control and model groups. (C) Volcano plot of differentially expressed lncRNA in B4 *vs* model group. (D) GO enrichment analysis of control and model groups. (E) GO enrichment analysis of B4 and model groups. (F) KEGG enrichment analysis of control and model groups. (G) KEGG enrichment analysis of B4 and model groups. (H) qPCR was used to detect the expression of downstream mRNA of differentially expressed lncRNAs. (I) The binding position of B4 with key proteins NLRP3, NF-κB and iNOS. Data are presented as means ± SD (n = 5). $^{\#}P < 0.05$, $^{\#\#}P < 0.01$, $^{\#\#\#}P < 0.001$ *vs* Control group; $^{*}P < 0.05$, $^{**}P < 0.01$, $^{***}P < 0.001$ *vs* MSU group.

($P < 0.05$, Fig. 3A). In addition, for THP-1 cells stimulated by MSU, B4 also effectively inhibited the mRNA expression of inflammatory factors such as *IL-1β*, *PGE2* and *TNF-α* ($P < 0.05$, Fig. 3B). Subsequently, the results were further verified by Western blot, and it was confirmed that B4 had a significant inhibitory effect on the expression of NLRP3 inflammasome components and related proteins. Specifically, B4 could effectively inhibit the expression of NLRP3, ASC, Caspase-1 and IL-1β in THP-1 cells ($P < 0.05$, Figs. 4A–4E). It is worth noting that NF-κB is a key regulator of various pro-inflammatory cytokines such as IL-1β, PGE 2 and TNF-α.Therefore, we explored whether B4 can also regulate NF-κB signaling pathway. Consistent with the expected results, B4 significantly reduced the expression of p-NF-κB protein in THP-1 cells treated with MSU (Figs. 4F–4G). Based on all the experimental results, B4 can inhibit the activation of NLRP3 inflammasome, thereby weakening the subsequent inflammatory cascade and its downstream effects. Finally, B4 could inhibit the inflammatory response of THP-1 cells induced by MSU.

3.5. B4 inhibits MSU-induced M1 polarization in THP-1 macrophages

This M1 polarization phenomenon occurs in the early stage of the GA model. In order to explore whether B4 treatment can inhibit M1 polarization by down-regulating the expression of these markers, we used CD80 and CD86 as established M1 macrophage polarization biomarkers for detection. As shown in Fig. 5A, compared with the normal control group, the mRNA expression levels of CD80 and CD86 in the model group were significantly increased, and the difference was statistically significant. However, when comparing the B4 treatment group with the model group, the MSU-induced increase in CD80 and CD86 mRNA expression was significantly inhibited by B4. M1 macrophages can secrete a large number of pro-inflammatory cytokines (IL-6) and play a key role in antigen presentation. The experimental results also showed that compared with the model group, IL-6 in the B4 treatment group was significantly reduced, confirming that B4 could effectively inhibit IL-6 secretion. To further explore whether the anti-inflammatory effect of B4 is mediated by inhibiting macrophage polarization, we used flow cytometry to detect the expression level of CD80 in THP-1 cells. Flow cytometry analysis showed that the level of CD80 in the MSU-treated model group was significantly higher than that in the untreated control group. On the contrary, all B4 treatment groups showed a dose-dependent decrease in CD80 levels compared with the MSU model group (Figs.5B–5C), and there were statistically significant differences between the dose groups. These results indicate that B4 can effectively inhibit the expression of M1 macrophage marker CD80 in THP-1 cells induced by MSU.

iNOS protein, which is involved in inflammatory response and immune defense, is also a marker of M1 macrophage polarization. As shown in Figs.5D and 5E, the iNOS protein level in the model group was significantly higher than that in the control group. In contrast, the expression of iNOS in the B4 treatment group was significantly reduced ($P < 0.05$), showing a statistically significant difference.Taken together, these results clearly confirm that B4 can inhibit MSU-induced M1 macrophage polarization in THP-1 cells. In summary, our results demonstrate that B4 can effectively inhibit MSU-induced M1 macrophage polarization in THP-1 cells.

3.6. Effect of B4 on NLRP3 inflammatory expression in MSU-induced GA mice

In order to verify the results of previous studies, we used MSU-induced GA mouse model to evaluate the effect of drug B4 on NLRP3, inflammasome and M1 macrophage polarization. QPCR analysis showed that compared with the normal control group without any treatment, the mRNA expression levels of markers reflecting inflammatory signals (such as *NLRP3*, *IL-1β*, *TNF-α* and *PGE2*) in the MSU model group were significantly increased and showed a significant upward trend. On the other hand, compared with the model group, the mRNA levels of all the treatment groups receiving B4 were significantly reduced, and the degree of reduction was statistically significant (Fig. 6A). Based on the above results, it can be concluded that B4 can effectively inhibit

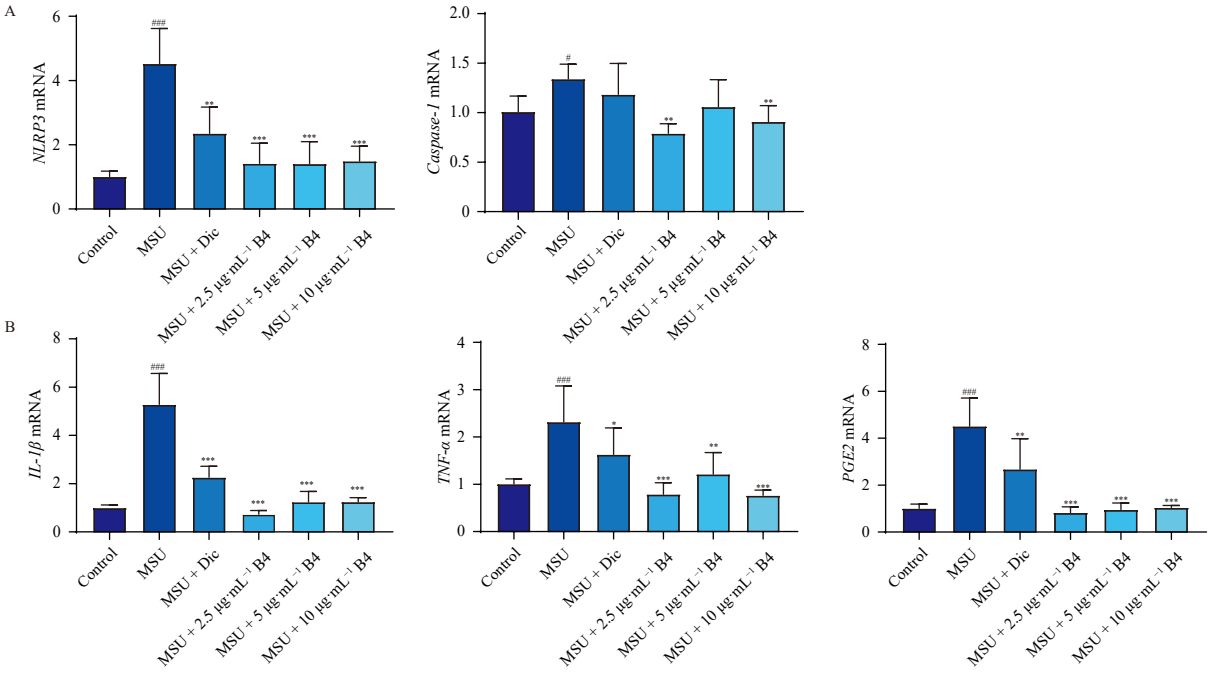

Fig. 3 B4 inhibits the expression of NLRP3 inflammasome-related mRNA in THP-1 cells induced by MSU. (A) Expression of NLRP3 inflammatory associated mRNA by qPCR. (B) qPCR detection of inflammatory factor mRNA expression. Data are presented as means ± SD (n = 3). $^{\#}P < 0.05$, $^{\#\#}P < 0.01$, $^{\#\#\#}P < 0.001$ *vs* Control group; $^{*}P < 0.05$, $^{**}P < 0.01$, $^{***}P < 0.001$ *vs* MSU group.

the expression of NLRP3 inflammasome-related messenger RNA in MSU-induced GA mice.

Subsequently, we used Western blotting for further analysis, and the results confirmed that B4 could inhibit the expression of NLRP3 inflammasome-related proteins. Specifically, the protein levels of p-NF-κB p65, NLRP3, Caspase-1 and ASC in the ankle tissue of the model group were significantly increased ; after using B4, the expression levels of these proteins (p-NF-κB p65, NLRP3, ASC and Caspase-1) in ankle joint tissues were significantly decreased ($P < 0.05$; Figs. 6B–6G). In summary, these results indicate that B4 can inhibit NLRP3 inflammasome, thereby inhibiting MSU-induced inflammatory response. Therefore, the downstream inflammatory cascade triggered by MSU crystals is also weakened. Based on all the above findings, it is clear that B4 can inhibit the polarization of M1 macrophages in THP-1 cells induced by MSU.

3.7. Effect of B4 on MSU-induced polarization of M1 macrophages in GA mice

In order to explore the effect of B4 on the phenotypic changes of macrophages induced by MSU in the ankle joint of GA mice, we

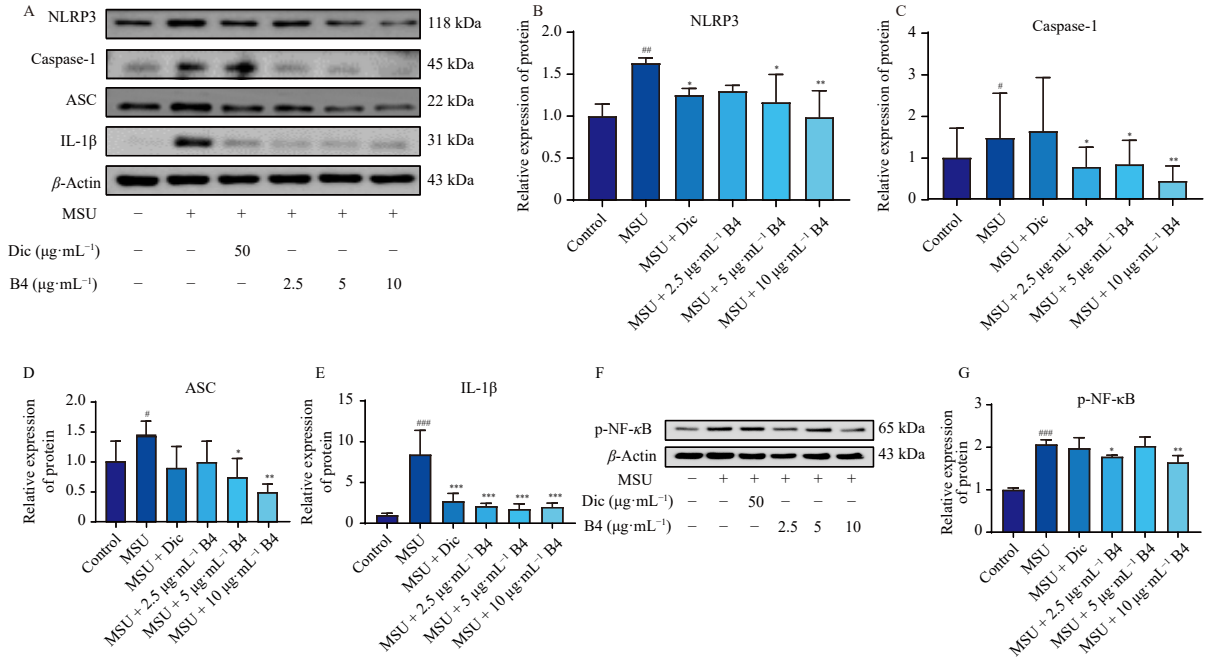

Fig. 4 B4 inhibits the expression of NLRP3 inflammasome-related proteins in THP-1 cells induced by MSU. (A) Western blot for the expression of NLRP3, ASC, Caspase-1, and IL-1β proteins. (B) Gray scale analysis of NLRP3. (C) Gray scale analysis of Caspase-1. (D) Gray scale analysis of ASC. (E) Gray scale analysis of IL-1β. (F) Western blot detection of p-NF-κB protein expression. (G) Gray scale analysis of p-NF-κB. Data are presented as means ± SD (n = 3). $^{\#}P < 0.05$, $^{\#\#}P < 0.01$, $^{\#\#\#}P < 0.001$ *vs* Control group; $^{*}P < 0.05$, $^{**}P < 0.01$, $^{***}P < 0.001$ *vs* MSU group.

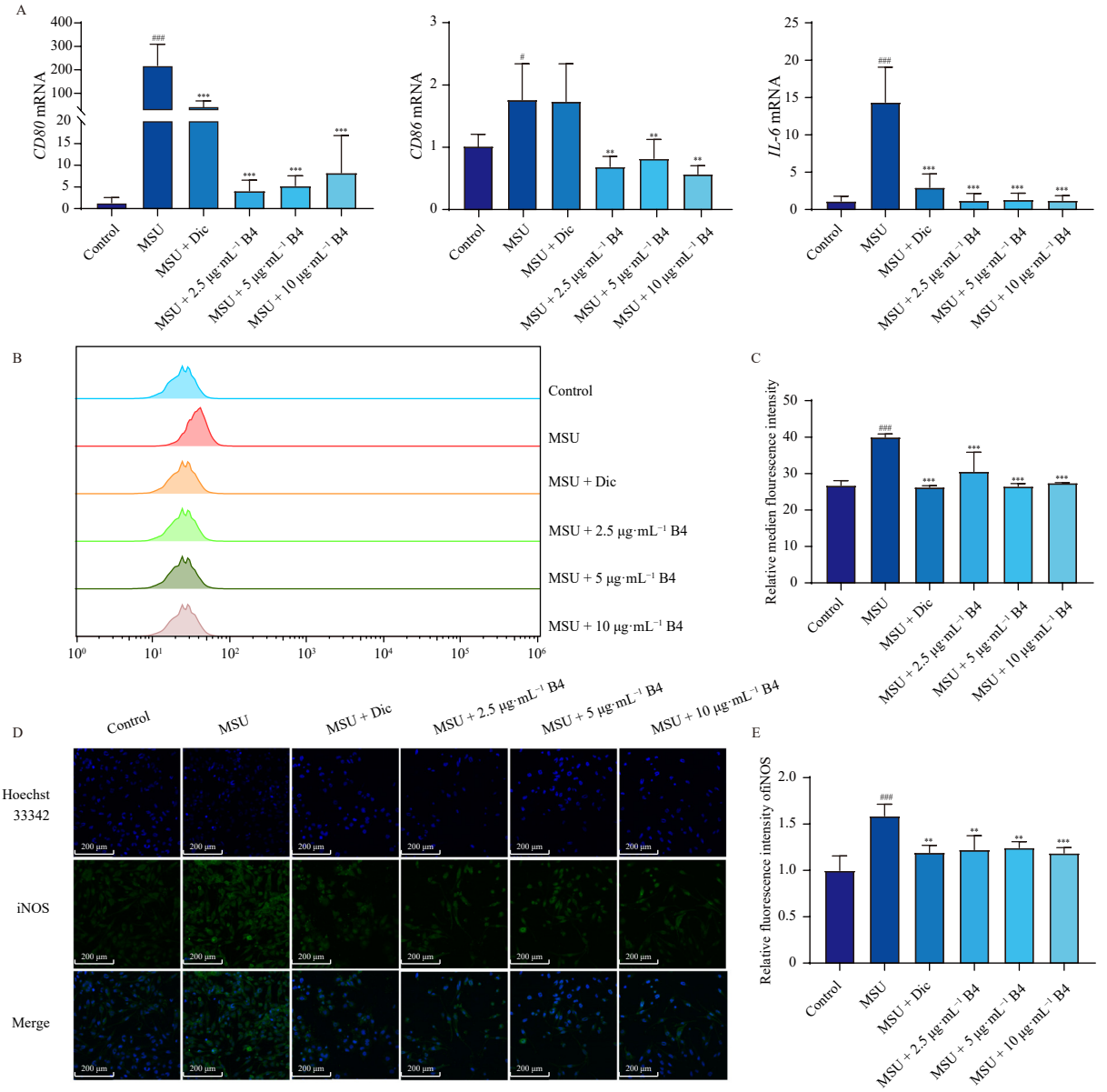

Fig. 5 B4 inhibited MSU-induced activation of M1 macrophage polarization in THP-1 cells. (A) qPCR detection of macrophage M1 polarization-associated m RNA expression. (B) Flow cytometry analysis of CD80 expression. (C) Expression level of CD80 fluorescence intensity. (D) Immunofluorescence detection of iNOS expression. (E) Fluorescence intensity analysis of iNOS. Data are presented as means ± SD (n = 3). $^{\#}P < 0.05$, $^{\#\#}P < 0.01$, $^{\#\#\#}P < 0.001$ *vs* Control group; $^{*}P < 0.05$, $^{**}P < 0.01$, $^{***}P < 0.001$ *vs* MSU group.

analyzed the expression of M1 macrophage polarization-related mRNA in ankle joint tissue. The results of qPCR showed that the expression of *iNOS*, *CD80* and *CD86* mRNA (M1 polarization markers) was significantly up-regulated in the MSU model group compared with the control group. On the contrary, the expression of *iNOS*, *CD80* and *CD86* mRNA in all B4 treatment groups was significantly down-regulated compared with the MSU model group (Fig. 7A). In addition, we detected the expression of iNOS protein (M1 macrophage marker) in ankle tissue of GA mice. As shown in Figs.7B–7C, the level of iNOS protein in the ankle joint of the model group was significantly higher than that of the control group.

Compared with the model group, the expression level of iNOS protein in ankle joint tissue was significantly decreased after B4 treatment. On the other hand, the polarization state of M1 macrophages was observed by immunofluorescence analysis. In GA synovial tissue, the proportion of iNOS positive area was significantly higher than that in the control group. However, after B4 treatment, the proportion of iNOS positive areas in synovial tissue decreased significantly (Figs.7D–7E). By integrating and summarizing all the experimental results, the following conclusions can be drawn: B4 can reduce the expression of inducible nitric oxide synthase (iNOS) in synovial macrophages, thereby inhibiting the polarization process of M1 macrophages. Comprehensive analysis of these experimental data can clearly confirm that B4 can indeed inhibit the polarization of M1 macrophages induced by MSU in the ankle joint of mice (Fig. 8).

4. Discussions

Gout is a metabolic disorder characterized by hyperuricemia and the deposition of MSU crystals. When serum uric acid levels exceed the saturation threshold, MSU crystals form and deposit in joints, triggering activation of resident macrophages. This process elicits local inflammatory responses and tissue damage, ultimately leading to the development of GA [16]. Macrophages act as key mediators in GA pathogenesis, serving as central components of innate immunity. When deposited in joints and adjacent tissues, MSU crystals are recognized and phagocytosed by resident macrophages *via* Toll-like receptors (TLRs), triggering neut-

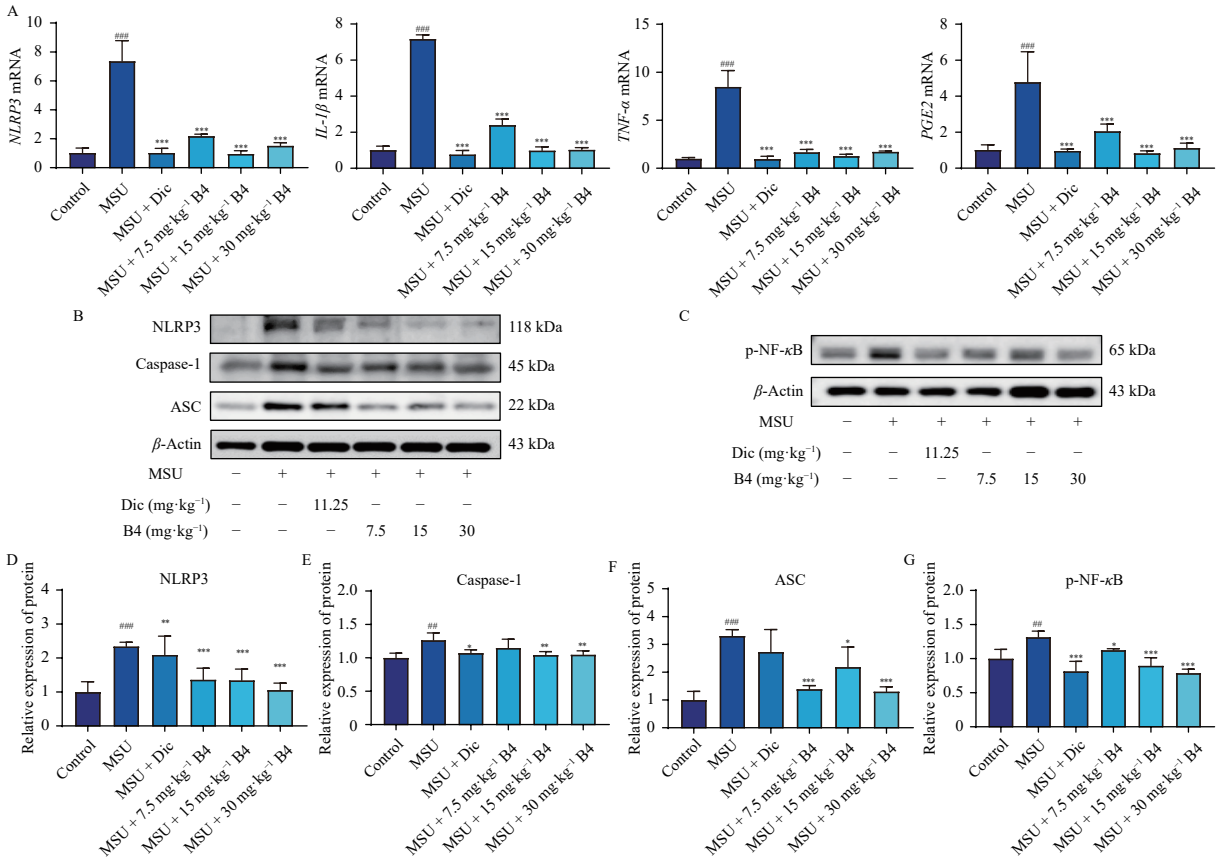

Fig. 6 B4 inhibits MSU-induced activation of NLRP3 inflammatory in GA mice. (A) qPCR detection of NLRP3 inflammatory with associated inflammatory factor mRNA expression. (B) Western blot detection of NLRP3, ASC, Caspase-1,protein expression. (C) Western blot detection of p-NF-κB protein expression. (D) Gray-scale analysis of NLRP3. (E) Gray-scale analysis of Caspase-1. (F) Gray-scale analysis of ASC. (G) Gray-scale analysis of p-NF-κB. Data are presented as means ± SD (n = 3). $^{\#}P < 0.05$, $^{\#\#}P < 0.01$, $^{\#\#\#}P < 0.001$ *vs* Control group; $^{*}P < 0.05$, $^{**}P < 0.01$, $^{***}P < 0.001$ *vs* MSU group.

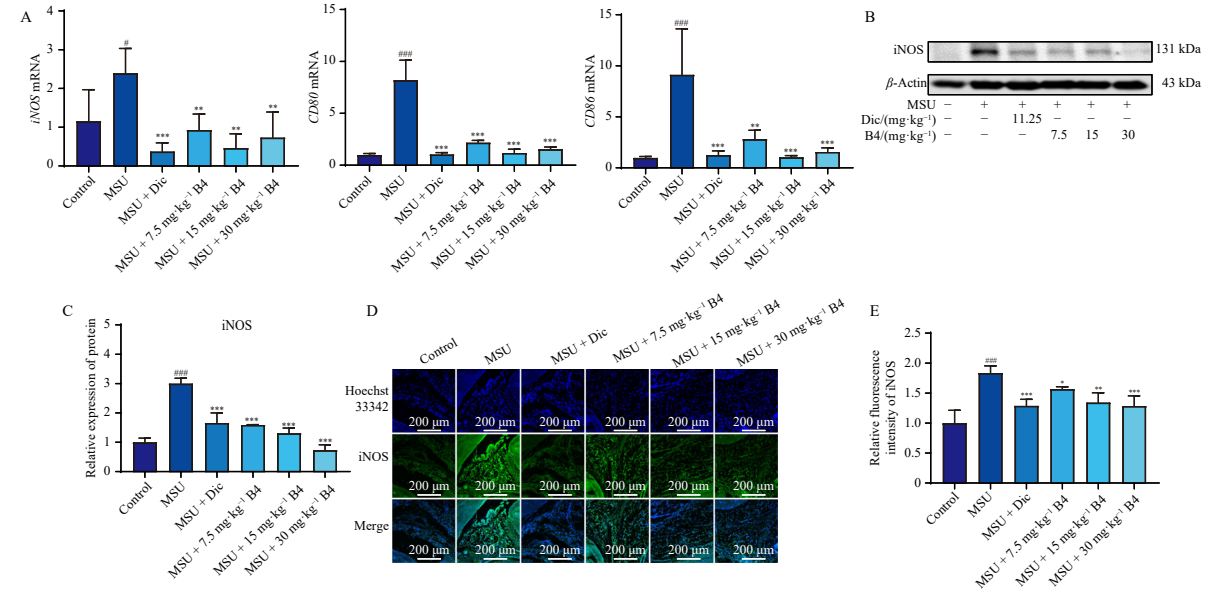

Fig. 7 B4 inhibits MSU-induced macrophage M1 polarization in gouty arthritis mice. (A) qPCR detection of macrophage M1 polarization-associated factor iNOS, CD80, CD86 mRNA expression. (B) Western blot detection of iNOS protein expression. (C) Gray-scale analysis of iNOS. (D) Immunofluorescence to detect the expression of iNOS fluorescence intensity. (E) Fluorescence intensity analysis of iNOS. Data are presented as means ± SD (n = 3). $^{\#}P < 0.05$, $^{\#\#}P < 0.01$, $^{\#\#\#}P < 0.001$ *vs* Control group; $^{*}P < 0.05$, $^{**}P < 0.01$, $^{***}P < 0.001$ *vs* MSU group.

rophilic inflammation and recruiting additional macrophages. Moreover, M1-polarized macrophages release abundant reactive nitrogen/oxygen species and pro-inflammatory cytokines, driving inflammatory progression, inducing endothelial cell injury, and initiating an amplified inflammatory cascade [17]. Numerous studies [18–21] have confirmed the involvement of multiple cell signaling pathways in GA pathogenesis, including the NF-κB signaling pathway, NLRP3 inflammasome-related pathways, and adenosine triphosphate (ATP)-gated purinergic ion channels. Future research may focus on investigating additional signaling path-

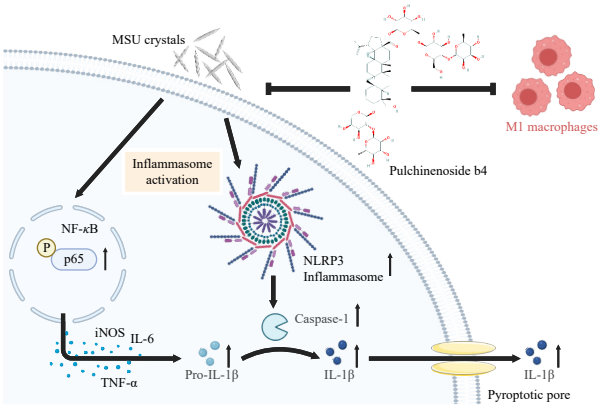

Fig. 8 Schematic illustration of B4's mechanism in ameliorating GA *via* regulation of the NLRP3 inflammasome and macrophage polarization. B4 alleviates GA by suppressing NF-κB signaling, inhibiting NLRP3 inflammasome activation, reducing IL-1β secretion, and blocking MSU-induced M1 macrophage polarization.

ways and targeting key components within these networks, which could potentially identify novel therapeutic targets for exploring B4's application in GA treatment.

In the traditional Chinese medicine treatment system, its core concept is mainly reflected in the holistic view and syndrome differentiation and treatment [22]. The theory regards the human body as a whole system, and achieves the treatment goal by harmonizing the balance of yin and yang and promoting the operation of qi and blood [23]. The advantage of traditional Chinese medicine is that it has a multi-target treatment strategy and relatively mild side effects. On the one hand, it emphasizes the development of personalized treatment programs for patients. On the other hand, it can show unique efficacy in dealing with chronic and difficult diseases [24]. B4 is compound extracted from *Pulsatilla chinensis* [25]. As a triterpenoid saponin compound, B4 has many functions such as anti-tumor, anti-inflammatory, anti-virus, kidney protection, analgesia and immune regulation [26]. Studies have confirmed that [27] B4 can inhibit the release of inflammatory factors by regulating the signal axis composed of myosin light chain kinase (MLCK)/phosphorylated myosin light chain-2 (p-MLC2)/NLRP3 inflammasome, thereby exerting a therapeutic effect on colitis. In addition, B4 (2.5, 5 or 10 mg·kg^{-1}) can also inhibit the release of inflammatory mediators by regulating the TLR4/NF-κB pathway, and has a significant improvement effect on lipopolysaccharide (LPS), Klebsiella pneumoniae and influenza virus FM1-induced pneumonia [28].

B4 is a triterpenoid saponin compound with multiple glycosidic bonds in its molecular structure. Since glycosides are prone to hydrolysis under acidic conditions and the gastrointestinal environment itself is acidic, the combined action of these two factors will lead to the hydrolysis of glycosidic bonds in B4. Therefore, B4 undergoes a significant degradation process before being absorbed into the body. This structural feature significantly limits the absorption of B4, which ultimately leads to its relatively low oral bioavailability. In the rat experiment, the maximum plasma concentration (C_{max} value) achieved by intraperitoneal injection of 122 mg·kg^{-1} B4 was 94.47 ± 28.99 ng·mL^{-1}; the C_{max} value can reach 10 394.16 ± 5041.38 ng·mL^{-1} , which is significantly higher. The C_{max} of enteric-coated capsules was 219.96 ± 103.32 ng·mL^{-1}. In terms of *in vivo* exposure levels, the area under the plasma curve (*AUC*) was 592.55 ± 57.78 ng·h·mL^{-1}. However, after rectal administration of B4 suppository, the *AUC* value of plasma could reach 29 115.16 ± 14 345.48 ng·h·mL^{-1}, which was about 49 times of the *AUC* value of oral B4 solution. The plasma *AUC* value of oral B4 enteric-coated capsules was measured to be 1049.00 ± 101.54 ng·h·mL^{-1}, which was about 1.77 times that of direct drinking B4 solution [29]. In this study, the pharmacokinetic method was used to systematically evaluate the plasma concentration-time curves of B4 in rats under different routes of administration (including intravenous injection, rectal suppository, oral enteric-coated capsules and direct drinking of B4 solution), and the corresponding pharmacokinetic parameters were calculated. The results showed that compared with direct oral administration of B4 solution, intravenous injection, rectal suppository and oral enteric-coated capsules could significantly shorten the peak time (*T*max) and improve the bioavailability of the drug [30–32]. It can be clearly seen from the pharmacokinetic studies of these B4 that different routes of administration can significantly affect the pharmacokinetic characteristics of the drug in rats. This finding can provide key guidance for how to choose the most appropriate route of administration and dosage form in the process of new drug research and development, and also provide scientific basis for subsequent clinical research. In addition, the rigorous design of this study can effectively improve the success rate of clinical trials and accelerate the transformation of laboratory research results into clinical applications.

Recent studies have deepened the understanding of the pathogenesis of GA. The pathological process of the disease has gradually become clear, revealing that it is the result of the interaction of multiple factors. Among them, uric acid metabolism disorder, NLRP3 inflammasome overactivation and oxidative stress injury are the key factors. In addition, the release of pro-inflammatory cytokines such as IL-1β and TNF-α is also involved. These factors work together. In this context, many traditional Chinese medicines and their bioactive components are considered to have multi-target regulation potential, which can alleviate the development of gout. At present, single cell RNA sequencing technology has been applied to the study of the pathogenesis of gout. Taking the rat arthritis model as an example, 932 differentially expressed long non-coding RNAs (lncRNAs) were identified by sequencing. Further analysis showed that the analgesic compound N^6-(2-hydroxyethyl) adenine extracted from *Cordyceps sinensis* could activate A1 adenosine receptor and inhibit A2A receptor. Through these two mechanisms, this substance can regulate multiple signaling pathways related to inflammatory response and ion channels, thereby achieving analgesic effect. This provides a promising new method for the treatment of gout [33]. Zhang et al. found that Huangqin Qingre Guanjie Capsule (HQC) can inhibit the PI3K/AKT signaling pathway by targeting the long-chain non-coding RNA (lncRNA) H19/APN axis, which can improve the lipid metabolism disorder and inflammatory response in patients with gout. This study elucidates the molecular mechanism of HQC's therapeutic effect through lncRNA H19/APN/PI3K/AKT pathway, and points out that lncRNA APN may become a future therapeutic target [34]. This study integrated transcriptomics and network pharmacology analysis to confirm that YGG can inhibit the TLR4/MYD88/NF-κB signaling pathway to alleviate the inflammatory response. Specifically, the phosphorylation level of p65 protein decreased, and the contents of IKKα/β and IκBα also decreased accordingly. These results indicate that YGG achieves therapeutic effects by acting on uric acid metabolism and inflammatory pathways through its active components. The mechanism discovery provides a theoretical basis for the application of YGG in clinical practice of gout under the guidance of traditional Chinese medicine theory [35]. In addition, our previous studies have confirmed that B4 has significant therapeutic potential for MSU-induced GA. It can quickly relieve joint swelling and fever symptoms and help restore foot function. This clearly shows that this study has important value. Therefore, in this study, we aimed to use transcriptomics technology for in-depth analysis to elucidate the mechanism of B4 alleviating GA.

In the field of transcriptomics, the core goal is to comprehensively analyze the dynamic changes of gene transcription in different cell environments [36, 37]. In this study, the mechanism of the effect of B4 treatment on the mechanism of GA was explored

by using transcriptomics technology. The specific research process includes systematic difference analysis of lncRNA . By comparing the blank group with the model group, lncRNAs with significant expression differences such as Nod1, Rbck1 and Nfkbib were identified. Pycard, Card9, Antxr1 and other differentially expressed lncRNAs were detected in the comparison between the model group and the B4 group. It is worth noting that the Nod1 protein encoded by this gene plays a key role because it can activate the pathogen recognition signaling pathway [38]. RBCK1 is an E3 ubiquitin ligase that promotes the degradation of NLRP3 protein through ubiquitination, thereby effectively inhibiting the assembly of inflammasomes. At the same time, it can also inhibit the release of pro-inflammatory cytokines including IL-1β and IL-18 [39]. On the other hand, Pycard protein, as a key adaptor protein, is mainly involved in the assembly process of inflammasome, including the formation of NLRP1/2/3/6 complex, AIM2 complex and IFI16 complex. The protein can participate in all the above biological processes and activate caspase-1 enzyme, and can also accelerate the maturation process of proinflammatory cytokines [40]. These lncRNA-mediated mechanisms work together to regulate the inflammatory cascade. Therefore, B4 has become a multi-target candidate drug for the treatment of GA, and subsequent analysis results have confirmed this view. Firstly, GO enrichment analysis of differentially expressed lncRNAs showed that they were significantly enriched in immune system processes and inflammatory response-related pathways. Secondly, through KEGG pathway analysis, multiple enrichment pathways were found, including NOD-like receptor signaling pathway, TNF signaling pathway, NF-κB signaling pathway, rheumatoid arthritis-related pathway and a variety of inflammation-related cytokine networks. Subsequently, we performed molecular docking experiments on the key targets of these pathways (NLRP3, p-NF-κB and iNOS) with B4, and the results showed that they had strong binding affinity, confirming that these molecules are involved in B4-mediated GA treatment. All pathways related to inflammatory stimulation were triggered, which further verified the consistency of the results of this transcriptome analysis with previous research conclusions [26, 41–43]. The key targets NLRP3, p-NF-κB and iNOS in the pathway were combined with B4 for molecular docking. The results showed that there was a strong binding affinity between them, which clearly indicated that they were indeed involved in the treatment of GA by B4. These pathways are related to the response triggered by inflammatory stimulation, and the results of this transcription analysis further confirm that they are consistent with previous studies.

In order to further explore the anti-inflammatory mechanism of B4 in the treatment of GA, this study verified its regulatory effect on the key targets of NOD-like receptor (NLR) signaling pathway. The NLR signaling pathway is a basic immune defense mechanism, and the NLRP3 inflammasome is closely related to the pathogenesis of GA and plays a central role in the progression of gouty arthritis [44–46]. MSU crystals are recognized by cytoplasmic pattern recognition receptors as endogenous risk signals in gout. This recognition triggers monocyte-macrophage activation and neutrophil recruitment, which in turn forms inflammasomes composed of ASC, caspase-1 and NLRP3. The complex activates caspase-1 and processes pro-IL-1β into a mature pro-inflammatory form IL-1β. Secreted IL-1β amplifies the inflammatory response by promoting the release of other inflammatory factors and drives the pathogenesis of GA [47–49]. It was observed in the *in vitro* and *in vivo* experimental models that compared with the control group, the mRNA expression levels of NLRP3, Caspase-1, ASC and IL-1β in the MSU group were significantly increased, and the up-regulation was significant. It is worth noting that the expression levels of these genes can be significantly reduced after B4 treatment, which clearly indicates that B4 has an inhibitory effect on the activation of NLRP3 inflammasome. Subsequently, this result was further verified by Western blotting analysis, and the experimental data were also supported. In the MSU-induced GA model, B4 can down-regulate the protein expression level related to NLRP3 inflammasome. Based on all the experimental results, it can be concluded that B4 alleviates GA symptoms by inhibiting the NLRP3 inflammasome pathway.

MSU crystals form a complex with CD14, which is recognized by macrophages through binding to TLR2 and TLR4, leading to phagocytosis and MyD88-mediated activation of the NF-κB signaling pathway [50]. NF-κB stimulates the release of inflammatory factors such as cyclooxygenase-2 (COX-2), TNF-α and IL-6, and plays a critical role in GA in concert with NLRP3 inflammatory vesicles [51-53]. Thus, we investigated key targets including NF-κB, TNF-α, and IL-6. Results showed that MSU crystal stimulation up-regulated TNF-α and IL-6 mRNA expression in both cellular and murine models. In contrast, B4 treatment significantly suppressed TNF-α and IL-6 mRNA levels. Additionally, B4 markedly inhibited pNF-κB protein expression. Collectively, these findings indicate that B4 suppresses NF-κB signaling pathway activation by modulating NF-κB, TNF-α, and IL-6 expression.

At present, we know that the activation of NF-κB and NLRP3 inflammasome is closely related to the polarization of macrophages to M1 phenotype [54]. On the one hand, Wang et al. [55] reported that the expression of NLRP3 was significantly up-regulated in GA rat model and synovial cells induced by MSU crystals. In this model, if the expression level of NLRP3 inflammasome is high, it will promote the polarization of macrophages to pro-inflammatory M1 phenotype. On the other hand, the activation of NF-κB also plays a key role in inducing M1 macrophage polarization. If the NF-κB signaling pathway is inhibited, the polarization of the M1 phenotype can be inhibited, thereby delaying the progression of GA inflammation [56, 57]. Another study [58] showed that MSU could significantly up-regulate the expression of SFRP2 in mice by destroying the interaction of Wnt/β-catenin-p65, promote the nuclear translocation of NF-κB p65 subunit and enhance its transcriptional activity, thus promoting the polarization of macrophages in GA mice to pro-inflammatory M1 phenotype. In addition, silencing SFRP2 gene expression in GA mice can inhibit the infiltration of inflammatory cells in synovial tissue, inhibit the polarization of M1 macrophages, and reduce ankle swelling and endothelial injury. This study suggests that B4 may regulate the polarization of macrophages by regulating the NF-κB signaling pathway and NLRP3 inflammasome, thereby exerting an anti-inflammatory effect on MSU-induced GA. It is known that M1 macrophages have the characteristics of high expression of CD40, CD64, CD68, CD80, CD86 and human leukocyte antigen-DR [59]. Among them, CD80 and CD86, as co-stimulatory molecules, are expressed when M1 macrophages receive activation signals [60] and can respond to pathogen stimulation signals [61]. In this study, we observed that B4 significantly inhibited the expression of M1 polarization markers CD80, CD86 and iNOS, and reduced ankle swelling.It also alleviated the inflammatory response induced by GA in mice, confirming the role of B4 in regulating the polarization of M1 macrophages.

In summary, this study demonstrates the therapeutic potential of B4 in GA, with its core mechanism likely involving dual regulation of inflammatory pathways. Transcriptomic analysis strongly indicates that B4 targets the NLRP3 inflammasome for inhibition—a key molecular platform for sensing danger signals like MSU crystals. Activation of the NLRP3 inflammasome drives caspase-1 cleavage, promoting maturation and release of the potent pro-inflammatory cytokines IL-1β and IL-18, which are central to acute inflammation and tissue damage in GA. Thus, B4-mediated inhibition of the NLRP3 inflammasome effectively disrupts this key inflammatory cascade, addressing the inflammatory storm in GA at its source. Additionally, our findings show that B4 significantly suppresses MSU crystal-induced macrophage po-

larization toward the pro-inflammatory M1 phenotype, as evidenced by reduced expression of M1 polarization markers. M1 macrophages infiltrate GA lesions in large numbers, continuously secreting pro-inflammatory factors (such as TNF-α, IL-6, PGE2 and nitric oxide) to exacerbate inflammatory responses and tissue destruction. By inhibiting M1 polarization, B4 regulates macrophage immune function, promoting a shift from a pro-inflammatory to anti-inflammatory/repair phenotypes, thereby ameliorating the local inflammatory microenvironment. Thus, B4 likely exerts synergistic effects: 1) inhibiting NLRP3 inflammasome activation to block initiation of the core inflammatory signaling pathway and release of key cytokines; and 2) suppressing M1 macrophage polarization to reduce continuous production of pro-inflammatory mediators. These actions work in concert to effectively alleviate GA-induced inflammation and tissue damage. Notably, this study has certain limitations. Future research will utilize integrated multi-omics analysis and gene-editing technologies to confirm whether B4 alleviates GA pathogenesis by inhibiting NLRP3 inflammasome activation and subsequent macrophage M1 polarization.

Funding

This work was supported by the National Natural Science Foundation of China (Nos. 82204590 and 82560758), Jiangxi Provincial Natural Science Foundation (Nos. 20224BAB216099 and 20252BAC240467), China Postdoctoral Science Foundation (No. 2023M731439), Key Technologies R & D Programme of Nanchang City (No. 2024zdxm023), and Jiangxi University of Chinese Medicine Science and Technology Innovation Team Development Program (No. CXTD22001).

Declaration of competing interests

These authors have no conflict of interest to declare.

References

1 Dalbeth N, Gosling AL, Gaffo A, et al. Gout. *Lancet*. 2021;397(10287):1843-1855. https://doi.org/10.1016/S0140-6736(21)00569-9.
2 Patel U, Rajasingh S, Samanta S, et al. Macrophage polarization in response to epigenetic modifiers during infection and inflammation. *Drug Discov Today*. 2017;22(1):186-193. https://doi.org/10.1016/j.drudis.2016.08.006.
3 Lin S, Hu X, Li Y, et al. Stefin B alleviates the gouty arthritis in mice by inducing the M2 polarization of macrophages. *Naunyn Schmiedebergs Arch Pharmacol*. 2024;397(8):5677-5688. https://doi.org/10.1007/s00210-023-02911-w.
4 Zhou Q, Sun HJ, Zhang XW. Total saponin fraction of *Dioscorea nipponica* Makino improves gouty arthritis symptoms in rats *via* M1/M2 polarization of monocytes and macrophages mediated by arachidonic acid signaling. *Chin J Integr Med*. 2023;29(11):1007-1017. https://doi.org/10.1007/s11655-022-3729-y.
5 Liu L, Zhu XX, Zhao TY, et al. Sirt1 ameliorates monosodium urate crystal-induced inflammation by altering macrophage polarization *via* the PI3K/Akt /STAT6 pathway. *Rheumatology (Oxford)*. 2019;58(9):1674-1683. https://doi.org/10.1093/rheumatology/kez165.
6 Qin DE, Liang W, Yu Y, et al. Modified Simiaowan prevents and treats gouty arthritis *via* the Nrf2/NLRP3 inflammasome signaling pathway. *J Ethnopharmacol*. 2024;318(Pt A):116906. https://doi.org/10.1016/j.jep.2023.116906.
7 Wu YY, Zhou JW, Zuo XC, et al. Yanggan Jiangmei Formula alleviates hepatic inflammation and lipid accumulation in non-alcoholic steatohepatitis by inhibiting the NF-κB/NLRP3 signaling pathway. *Chin J Nat Med*. 2024;22(3):224-234. https://doi.org/10.1016/S1875-5364(24)60595-9.
8 Lin XY, Shao TJ, Huang L, et al. Simiao Decoction alleviates gouty arthritis by modulating proinflammatory cytokines and the gut ecosystem. *Front Pharmacol*. 2020;11:955. https://doi.org/10.3389/fphar.2020.00955.
9 Fan WM, Chen SX, Wu XH, et al. Resveratrol relieves gouty arthritis by promoting mitophagy to inhibit activation of NLRP3 inflammasomes. *J Inflamm Res*. 2021;14:3523-3536. https://doi.org/10.2147/JIR.S320912.
10 Cao L, Zhao TY, Xue Y, et al. The anti-inflammatory and uric acid lowering effects of Si-Miao-San on gout. *Front Immunol*. 2022;12:777522. https://doi.org/10.3389/fimmu.2021.777522.
11 Luo ZW, Yin FF, Wang XB, et al. Progress in approved drugs from natural product resources. *Chin J Nat Med*. 2024;22(3):195-211. https://doi.org/10.1016/S1875-5364(24)60582-0.
12 Gong Q, Yin JL, Wang ML, et al. Anemoside B4 exerts hypoglycemic effect by regulating the expression of GLUT4 in HFD/STZ rats. *Molecules*. 2023;28(3):968. https://doi.org/10.3390/molecules28030968.
13 Yuan RYK, He J, Huang LT, et al. Anemoside B4 protects against acute lung injury by attenuating inflammation through blocking NLRP3 inflammasome activation and TLR4 dimerization. *J Immunol Res*. 2020;7502301. https://doi.org/10.1155/2020/7502301.
14 Ma HM, Zhou MJ, Duan WB, et al. Anemoside B4 prevents acute ulcerative colitis through inhibiting of TLR4/NF-κB/MAPK signaling pathway. *Int Immunopharmacol*. 2020;87:106794. https://doi.org/10.1016/j.intimp.2020.106794.
15 Liu Y, Grimm M, Dai WT, et al. CB-Dock: a web server for cavity detection-guided protein-ligand blind docking. *Acta Pharmacol Sin*. 2020;41(1):138-144. https://doi.org/10.1038/s41401-019-0228-6.
16 Zeng XJ, Zhang Y. The interpretation of 2018 updated European League Against Rheumatism evidence based recommendations for the diagnosis of gout. *Chin J Intern Med*. 2019;58(10):745-750. https://doi.org/10.3760/cma.j.issn.0578-1426.2019.10.005.
17 So AK, Martinon F. Inflammation in gout: mechanisms and therapeutic targets. *Nat Rev Rheumatol*. 2017;13(11):639-647. https://doi.org/10.1038/nrrheum.2017.155.
18 Wu MM, Tian Y, Wang QQ, et al. Gout: a disease involved with complicated immunoinflammatory responses: a narrative review. *Clin Rheumatol*. 2020;39(10):2849-2859. https://doi.org/10.1007/s10067-020-05090-8.
19 Cunningham CC, Corr EM, McCarthy GM, et al. Intra-articular basic calcium phosphate and monosodium urate crystals inhibit anti-osteoclastogenic cytokine signalling. *Osteoarthritis Cartilage*. 2016;24(12):2141-2152. https://doi.org/10.1016/j.joca.2016.07.001.
20 Funes SC, Rios M, Escobar-Vera J, et al. Implications of macrophage polarization in autoimmunity. *Immunology*. 2018;154(2):186-195. https://doi.org/10.1111/imm.12910.
21 Liu YZ, Tang HL, Liu XX, et al. Frontline science: reprogramming COX-2, 5-LOX, and CYP4A-mediated arachidonic acid metabolism in macrophages by salidroside alleviates gouty arthritis. *J Leukoc Biol*. 2019;105(1):11-24. https://doi.org/10.1002/JLB.3HI0518-193R.
22 Li YX, Yuan JB, Deng W, et al. Buqi-Tongluo Decoction inhibits osteoclastogenesis and alleviates bone loss in ovariectomized rats by attenuating NFATc1, MAPK, NF-κB signaling. *Chin J Nat Med*. 2025;23(1):90-101. https://doi.org/10.1016/S1875-5364(25)60810-7.
23 Yang WQ, Wen W, Chen H, et al. Zhongfeng Xingnao Liquid ameliorates post-stroke cognitive impairment through sirtuin1 (SIRT1)/nuclear factor erythroid 2-related factor 2 (Nrf2)/heme oxygenase 1 (HO-1) pathway. *Chin J Nat Med*. 2025;23(1):77-89. https://doi.org/10.1016/S1875-5364(25)60808-9.
24 Xu XJ, Long JB, Jin KY, et al. Danshen-Chuanxiongqin Injection attenuates cerebral ischemic stroke by inhibiting neuroinflammation *via* the TLR2/TLR4-MyD88-NF-κB pathway in tMCAO mice. *Chin J Nat Med*. 2021;19(10):772-783. https://doi.org/10.1016/S1875-5364(21)60083-3.
25 Zhang Y. Awareness and ability of paradigm shift are needed for research on dominant diseases of TCM. *Chin Herb Med*. 2023;15(4):475. https://doi.org/10.1016/j.chmed.2023.10.001.
26 Li YH, Zou M, Han Q, et al. Therapeutic potential of triterpenoid saponin anemoside B4 from *Pulsatilla chinensis*. *Pharmacol Res*. 2020;160:105079. https://doi.org/10.1016/j.phrs.2020.105079.
27 Feng W, Zhang Y, Zhang YW, et al. Anemoside B4 ameliorates dextran sulfate sodium (DSS)-induced colitis through inhibiting NLRP3 inflammasome and modulating gut microbiota. *Eur J Pharmacol*. 2024;963:176164. https://doi.org/10.1016/j.ejphar.2023.176164.
28 He J, Yuan RYK, Cui XL, et al. Anemoside B4 protects against *Klebsiella pneumoniae*- and influenza virus FM1-induced pneumonia *via* the TLR4/Myd88 signaling pathway in mice. *Chin Med*. 2020;15:68. https://doi.org/10.1186/s13020-020-00350-w.
29 Ye Y. Pharmacokinetic study on the anti-hyperuricemia efficacy of Leukoderma saponin B4 and different administration routes. Nanning: University of Chinese Medicine in Guangxi; 2023. https://doi.org/10.27879/dcnki.ggxzy.2023.000665.
30 Zhou C. Study on the efficacy and pharmacokinetics of saponin B4 suppository in the treatment of chronic colitis. Nanchang: Jiangxi University of Traditional Chinese Medicine; 2021. https://doi.org/10.27180/d.cnki.gjxzc.2021.000245.
31 Ye YQ, Xue MZ, Tian XT, et al. Pharmacokinetic and metabolite profile of orally administered anemoside B4 in rats with an improved exposure in formulations of rectal suppository. *J Ethnopharmacol*. 2023;315:116694. https://doi.org/10.1016/j.jep.2023.116694.
32 Liu CY, Fu TT, Yang FF, et al. Comparative study on pulmonary pharmacokinetics and anti-inflammatory effects of *Pulsatilla* saponin B4 after tracheal and intravenous administration. *Acta Pharm Sin*. 2022;57(9):2791-2797. https://doi.org/10.16438/j.0513-4870.2022.0307.
33 Zhu W, Chai Y, Jin Y, et al. The effects of *Cordyceps sinensis* analgesic compounds on the transcriptome and pain-related genes such as *Adora1* in gout rats. *J Mycol*. 2017;36(1):48-59. https://doi.org/10.13346/j.mycosystema.160262.
34 Zhang XH, Liu J, Sun YQ, et al. Chinese herbal compound Huangqin Qingrechubi Capsule reduces lipid metabolism disorder and inflammatory response in gouty arthritis *via* the LncRNA H19/APN/PI3K/AKT cascade. *Pharm Biol*. 2023;61(1):541-555. https://doi.org/10.1080/13880209.2023.2191641.
35 Fan QQ, Zhai BT, Zhang D, et al. Study on the underlying mechanism of Yinhua Gout Granules in the treatment of gouty arthritis by integrating transcriptomics and network pharmacology. *Drug Des Devel Ther*. 2024;18:3089-3112. https://doi.org/10.2147/DDDT.S475442.
36 Liu SL, Wang XH, Gao YG, et al. Transcriptomic analysis identifies differentially expressed genes (DEGs) associated with bolting and flowering in *Saposhnikovia divaricata*. *Chin J Nat Med*. 2018;16(6):446-455. https://doi.

org/10.1016/S1875-5364(18)30078-5.
37 Geng QS, Liu RJ, Shen ZB, et al. Transcriptome sequencing and metabolome analysis reveal the mechanism of Shuanghua Baihe Tablet in the treatment of oral mucositis. *Chin J Nat Med*. 2021;19(12):930-943. https://doi.org/10.1016/S1875-5364(22)60150-X.
38 Gulzar F, Chhikara N, Kumar P, et al. ER stress aggravates NOD1-mediated inflammatory response leading to impaired nutrient metabolism in hepatoma cells. *Biochem Biophys Res Commun*. 2024;735:150827. https://doi.org/10.1016/j.bbrc.2024.150827.
39 Du JW, Peng LJ, Feng J, et al. RBCK1 overexpression attenuates inflammation and mobility of Derp1-induced nasal mucosal cells by downregulating NLRP3. *Int Arch Allergy Immunol*. 2023;184(5):471-480. https://doi.org/10.1159/000527962.
40 Yao Z, Li Y, Mai H, et al. Comprehensive multiomics analysis identifies *PYCARD* as a key pyroptosis-related gene in osteoarthritis synovial macrophages. *Front Immunol*. 2025;16:1558139. https://doi.org/10.3389/fimmu.2025.1558139.
41 Ouyang X, Li NZ, Guo MX, et al. Active flavonoids from *Lagotis brachystachya* attenuate monosodium urate-induced gouty arthritis *via* inhibiting TLR4/MyD88/NF-κB pathway and NLRP3 expression. *Front Pharmacol*. 2021;12:760331. https://doi.org/10.3389/fphar.2021.760331.
42 Latz E, Duewell P. NLRP3 inflammasome activation in inflammaging. *Semin Immunol*. 2018;40:61-73. https://doi.org/10.1016/j.smim.2018.09.001.
43 Lyu S, Ding RW, Liu P, et al. LC-MS analysis of serum for the metabolomic investigation of the effects of Pulchinenoside b4 administration in monosodium urate crystal-induced gouty arthritis rat model. *Molecules*. 2019;24(17):3161. https://doi.org/10.3390/molecules24173161.
44 Wang SH, Lei P, Feng Y, et al. Jinyinqingre Oral Liquid alleviates LPS-induced acute lung injury by inhibiting the NF-κB/NLRP3/GSDMD pathway. *Chin J Nat Med*. 2023;21(6):423-435. https://doi.org/10.1016/S1875-5364(23)60397-8.
45 Duez H, Pourcet B. Nuclear receptors in the control of the NLRP3 inflammasome pathway. *Front Endocrinol (Lausanne)*. 2021;12:630536. https://doi.org/10.3389/fendo.2021.630536.
46 Zhang XY, Liu YB, Deng GR, et al. A purified biflavonoid extract from *Selaginella moellendorffii* alleviates gout arthritis *via* NLRP3/ASC/Caspase-1 axis suppression. *Front Pharmacol*. 2021;12:676297. https://doi.org/10.3389/fphar.2021.676297.
47 Zhang YZ, Sui XL, Xu YP, et al. NLRP3 inflammasome and lipid metabolism analysis based on UPLC-Q-TOF-MS in gouty nephropathy. *Int J Mol Med*. 2019;44(1):172-184. https://doi.org/10.3892/ijmm.2019.4176.
48 Broz P. Immunology: caspase target drives pyroptosis. *Nature*. 2015;526(7575):642-643. https://doi.org/10.1038/nature15632.
49 Wu C, Li F, Zhang X, et al. (−)-Epicatechin ameliorates monosodium urate-induced acute gouty arthritis through inhibiting NLRP3 inflammasome and the NF-κB signaling pathway. *Front Pharmacol*. 2022;13:799552. https://doi.org/10.3389/fphar.2022.799552.
50 Teng L, Shen Y, Qu YH, et al. Cyasterone inhibits IL-1β-mediated apoptosis and inflammation *via* the NF-κB and MAPK signaling pathways in rat chondrocytes and ameliorates osteoarthritis *in vivo*. *Chin J Nat Med*. 2023;21(2):99-112. https://doi.org/10.1016/S1875-5364(23)60388-7.
51 Schroder K, Tschopp J. The inflammasomes. *Cell*. 2010;140(6):821-832. https://doi.org/10.1016/j.cell.2010.01.040.
52 Yang G, Lee HE, Moon SJ, et al. Direct binding to NLRP3 pyrin domain as a novel strategy to prevent NLRP3-driven inflammation and gouty arthritis. *Arthritis Rheumatol*. 2020;72(7):1192-1202. https://doi.org/10.1002/art.41245.
53 Lin W, Shen P, Huang Y, et al. Wutou Decoction attenuates the synovial inflammation of collagen-induced arthritis rats *via* regulating macrophage M1/M2 type polarization. *J Ethnopharmacol*. 2023;301:115802. https://doi.org/10.1016/j.jep.2022.115802.
54 Wang L, Zhao M. Suppression of NOD-like receptor protein 3 inflammasome activation and macrophage M1 polarization by hederagenin contributes to attenuation of sepsis-induced acute lung injury in rats. *Bioengineered*. 2022;13(3):7262-7276. https://doi.org/10.1080/21655979.2022.2047406.
55 Tian J, Zhou D, Xiang L, et al. MiR-223-3p inhibits inflammation and pyroptosis in monosodium urate-induced rats and fibroblast-like synoviocytes by targeting NLRP3. *Clin Exp Immunol*. 2021;204(3):396-410. https://doi.org/10.1111/cei.13587.
56 Ma WT, Gao F, Gu K, et al. The role of monocytes and macrophages in autoimmune diseases: a comprehensive review. *Front Immunol*. 2019;10:1140. https://doi.org/10.3389/fimmu.2019.01140.
57 Fan B, Liu QY, Yang Y, et al. Soufeng Sanjie Formula alleviates osteoarthritis by inhibiting macrophage M1 polarization and modulating intestinal metabolites. *J Ethnopharmacol*. 2025;339:119147. https://doi.org/10.1016/j.jep.2024.119147.
58 Mei JT, Zhou F, Qiao H, et al. Nerve modulation therapy in gouty arthritis: targeting increased sFRP2 expression in dorsal root ganglion regulates macrophage polarization and alleviates endothelial damage. *Theranostics*. 2019;9(13):3707-3722. https://doi.org/10.7150/thno.33908.
59 Chen YN, Hu MR,Wang L, et al. Macrophage M1/M2 polarization. *Eur J Pharmacol*. 2020;877:173090. https://doi.org/10.1016/j.ejphar.2020.173090.
60 Cutolo M, Campitiello R, Gotelli E, et al. The role of M1/M2 macrophage polarization in rheumatoid arthritis synovitis. *Front Immunol*. 2022;13:867260. https://doi.org/10.3389/fimmu.2022.867260.
61 Sloas C, Gill S, Klichinsky M. Engineered CAR-macrophages as adoptive immunotherapies for solid tumors. *Front Immunol*. 2021;12:783305. https://doi.org/10.3389/fimmu.2021.783305.